

## Raman spectroscopy and effective dielectric function in PLZT $x/40/60$

This article has been downloaded from IOPscience. Please scroll down to see the full text article.

2008 J. Phys.: Condens. Matter 20 345229

(<http://iopscience.iop.org/0953-8984/20/34/345229>)

View [the table of contents for this issue](#), or go to the [journal homepage](#) for more

Download details:

IP Address: 129.252.86.83

The article was downloaded on 29/05/2010 at 14:36

Please note that [terms and conditions apply](#).

# Raman spectroscopy and effective dielectric function in PLZT $x/40/60$

E Buixaderas<sup>1</sup>, I Gregora<sup>1</sup>, S Kamba<sup>1</sup>, J Petzelt<sup>1</sup> and M Kosec<sup>2</sup>

<sup>1</sup> Institute of Physics, Academy of Sciences of the Czech Republic, Na Slovance 2, 18221 Prague, Czech Republic

<sup>2</sup> Jožef Stefan Institute, Jamova 39, 1000 Ljubljana, Slovenia

E-mail: [buixader@fzu.cz](mailto:buixader@fzu.cz)

Received 16 April 2008, in final form 3 July 2008

Published 7 August 2008

Online at [stacks.iop.org/JPhysCM/20/345229](http://stacks.iop.org/JPhysCM/20/345229)

## Abstract

The Raman spectra of the ceramics PLZT  $x/40/60$  have been measured in the temperature range 20–800 K. An assignment of the Raman modes is presented using the results of the effective medium approximation for the IR data. Factor-group analysis is presented for the case of off-site position of cations or unit cell doubling, which allows a higher number of active phonons in the IR and Raman spectra. The presence of Raman-active modes in the cubic phase is associated with local unit cell doubling and symmetry breakdown due to the off-site cations.

(Some figures in this article are in colour only in the electronic version)

## 1. Introduction

The exceptional optical and dielectric properties of the ceramic system  $(\text{Pb}_{1-3x/2}\text{La}_x)(\text{Zr}_y\text{Ti}_{1-y})\text{O}_3$  (PLZT $x/y/1-y$ ) have aroused considerable attention from the very beginning of its discovery [1, 2]. Many studies have been devoted to the origin of its relaxor behaviour [3–6]. The phase transition diagram of PLZT is very well known [1]. The morphotropic phase boundary between the tetragonal and rhombohedral symmetry is set for  $y = 53\%$  (amount of Zr). For  $y < 53\%$ , the tetragonal symmetry is realized at room temperature (RT). This side of the phase diagram has been less studied than the rhombohedral one: however, its dielectric properties are interestingly governed by the amount of La doping  $x$ , evolving from a traditional ferroelectric material at low La contents to a relaxor ferroelectric for  $x \geq 12\%$  [6]. This change in the dielectric behaviour was found to be associated with the polar domain sizes, reducing from micrometres in the ferroelectric case to nanometres in the relaxor one [7].

The first infrared (IR) and Raman spectra of PLZT 12/40/60 were published by Lurio *et al* [8] at RT and 200 °C. They tried to assign the mode symmetries according to those for  $\text{PbTiO}_3$ . However, they used the classical damped-oscillators model and the number of modes was not satisfactory to fully interpret the spectra. More recent Raman results were published by El Marshi *et al* for PLZT 12/40/60 and 6/40/60 [9, 10]. Despite the ceramic character of the samples, it was shown that selection rules

for the intensity of the Raman modes are applicable and they tried to again assign the mode symmetries, as already done for  $(\text{Pb}_{0.97}\text{Nd}_{0.02})(\text{Zr}_{0.55}\text{Ti}_{0.45})\text{O}_3$  [11]. Low-temperature Raman spectra and assignments of modes for different  $\text{Pb}(\text{Zr}_y\text{Ti}_{1-y})\text{O}_3$  (PZT) samples were also published by Frantti *et al* [12].

The lattice dynamics of ferroelectric PLZT 5/40/60 had already been studied by us using IR and dielectric spectroscopy [13]. It was shown that the dielectric behaviour of this sample, considered as a normal ferroelectric (with  $T_C = 584$  K), is governed by a soft mode in the THz range and a lower-frequency excitation related to polar microdomains appearing on lowering the temperature. The relaxor samples PLZT 12/40/60 and 15/40/60 were also studied very recently by us [14, 15]. We have found that the high-temperature overdamped excitation splits below  $T_C$  (400 and 300 K for  $x = 12$  and 15, respectively) into the E-symmetry soft mode, which hardens on further cooling, and a lower-frequency relaxation, which slows down further and broadens, as usual, in relaxor materials. Both samples show relaxor behaviour but undergo ferroelectric phase transitions, too. The huge dielectric anisotropy of PLZT 15/40/60 in the THz and IR range was recently evaluated using the effective medium approximation (EMA) [15]. This model shows that the cubic  $F_{1u}$  modes are already split into E and  $A_1$  tetragonal components above the ferroelectric phase transition due to the presence of polar clusters. XRD data of PLZT 12/40/60 showed that the off-site position of Pb/La atoms allows the activation of new IR-active modes in the tetragonal phase [15].

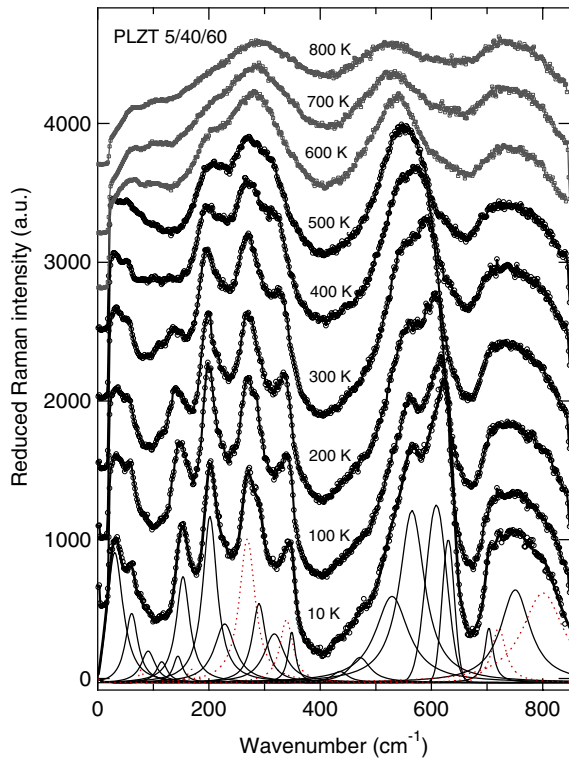


**Figure 1.** Raman spectra (corrected for the temperature factor) of PLZT 5/40/60 at selected temperatures. The fit at 10 K and the oscillators used in the fit are also shown. Dotted lines refer to purely Raman-active modes.

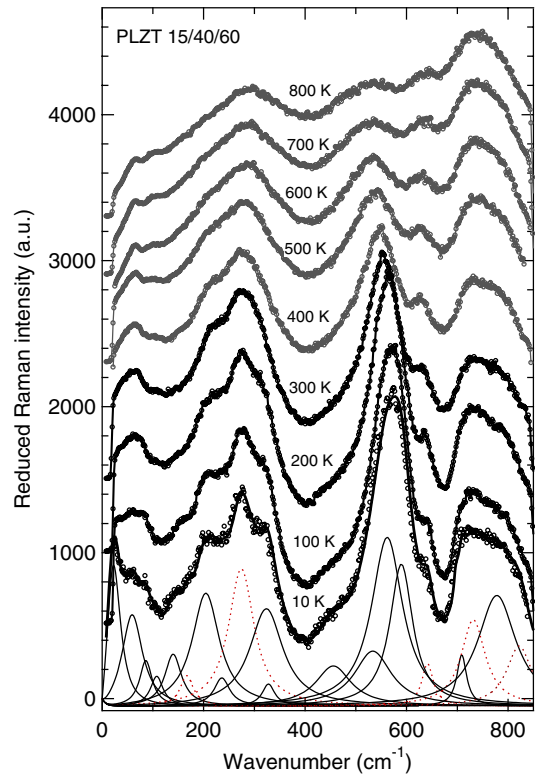


**Figure 2.** Raman spectra (corrected for the temperature factor) of PLZT 15/40/60 at selected temperatures. The fit at 10 K and the oscillators used in the fit are also shown. Dotted lines refer to purely Raman-active modes.

In the present paper we compare Raman and IR results for PLZT  $x/40/60$  samples:  $x = 5, 12$  and  $15$  at different temperatures. The EMA model is used to better understand the IR and Raman spectra and to be able to assign the mode symmetries.

## 2. Experimental details

The PLZT  $x/40/60$  ceramic samples were prepared by mixing an appropriate amount of p.a. grade oxides with 6 wt% PbO in excess. The powder mixture was calcined twice at 900 °C with intermediate milling. Further processing is described elsewhere [16]. According to x-ray diffraction (XRD) and scanning electron microscopy (SEM) analysis, the material was single-phase perovskite of high density. Large disc-like ceramics (diameter about 2 cm and 1.5 mm thick) were cut into discs (7 mm in diameter and 1 mm thick) to enable the IR and Raman measurements.

IR reflectivity measurements were performed using an FTIR spectrometer Bruker IFS 113v equipped with two RT DTGS pyroelectric detectors as well as an He-cooled (1.5 K) Si bolometer. RT and high-temperature spectra were taken in the range 30–3000  $\text{cm}^{-1}$  with a resolution of 2  $\text{cm}^{-1}$  and a DTGS pyroelectric detector. For high temperatures (300–900 K) a commercial oven SPECAC P/N 5850 was used. For low-temperature measurements (10–300 K) we used a continuous-flow Optistat CF (Oxford Instruments) cryostat with the sample mounted in an He gas bath. The use of polyethylene windows

in the cryostat reduced the accessible frequency range to 30–650  $\text{cm}^{-1}$  at low temperatures. Detection was done by an He-cooled (1.5 K) Si bolometer.

The Raman spectra were excited with the 514.5 nm line of an Ar laser at a power of several mW and recorded in back-scattering geometry using an RM-1000 Renishaw Raman microscope equipped with a grating filter, enabling good stray light rejection in the 20–850  $\text{cm}^{-1}$  range. The diameter of the laser spot on the sample surface amounted to 2–5  $\mu\text{m}$ . A THMS-600 cell (LINKAM) was used for temperature control of the samples from 300 to 800 K. For low-temperature spectra (between 300 and 10 K) samples were loaded into a continuous-flow He cryostat (Oxford Instruments) and the microscope was equipped with a special angled arm carrying a 20 $\times$  ULWD objective for efficient optical coupling. The spectral resolution was better than 2  $\text{cm}^{-1}$ .

## 3. Results

### 3.1. Raman results

The reduced Raman spectra (corrected for the Bose–Einstein temperature factor) of PLZT 5/40/60 and 15/40/60 at different temperatures are shown in figures 1 and 2. Spectra were recorded using the natural polarization of the laser without any analyser, which yields almost parallel polarization. The spectra are similar to those taken for PLZT 6/40/60 and 12/40/60 [10]. They show also the main features presented

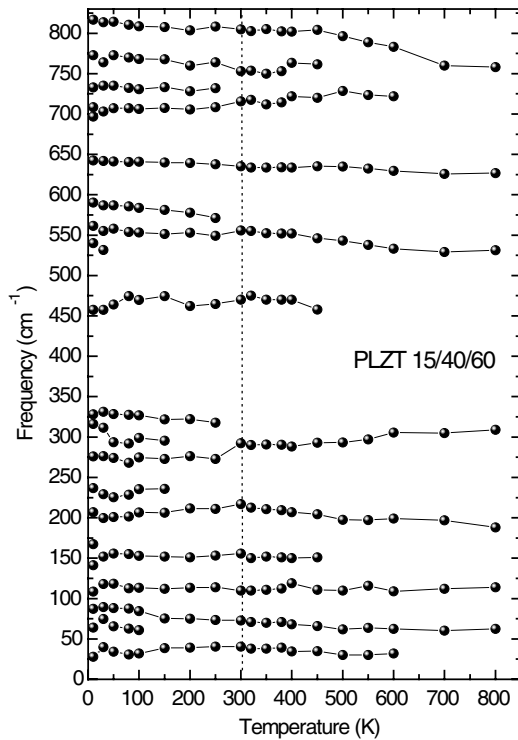


**Figure 3.** Temperature dependences of Raman frequencies for 15/40/60.

by PZT 30/70 [12]. Both compositions show similar peaks; however, closer inspection of the spectra shows that for PLZT 15/40/60 bands are broader at lower temperatures compared to PLZT 5/40/60. Also in PLZT 5/40/60 the splitting of the modes near  $550\text{ cm}^{-1}$  is more pronounced and the spectra are richer below  $400\text{ cm}^{-1}$ .

The fitting of the spectra was done using a sum of independent damped harmonic oscillators. However, in some cases the fitting of minima was difficult at the highest frequencies and Gaussian shapes were used for two bands in PLZT 5/40/60 near  $600\text{ cm}^{-1}$  at low temperatures. Fits for PLZT 5/40/60 and 15/40/60 at the lowest temperature and the corresponding peak decomposition are also shown in figures 1 and 2. Modes which are simultaneously IR-and Raman-active are shown by solid lines.

The temperature dependences of the Raman frequencies for PLZT 15/40/60 are shown in figure 3. (The temperature behaviour of the frequencies for PLZT 5/40/60 is shown afterwards, within the discussion section, with the assignments of symmetries.) The Raman signal is still present in the cubic phase, despite the forbidding selection rules, as it is well known for many cubic perovskites. Three main bands, which split on cooling, are seen. Particularly interesting is the splitting of the first band near  $300\text{ cm}^{-1}$  in the cubic phase because the first tetragonal  $A_1-E$  doublet, which is supposed to soften, develops from it on cooling. The second and third cubic bands near  $500$  and  $700\text{ cm}^{-1}$ , respectively, also develop some substructure. Besides these splittings, all the main peaks present some shoulders at the lowest temperatures.

An interesting feature is the presence of an intermediate peak, at  $\sim 640\text{ cm}^{-1}$ , which is stronger in samples with

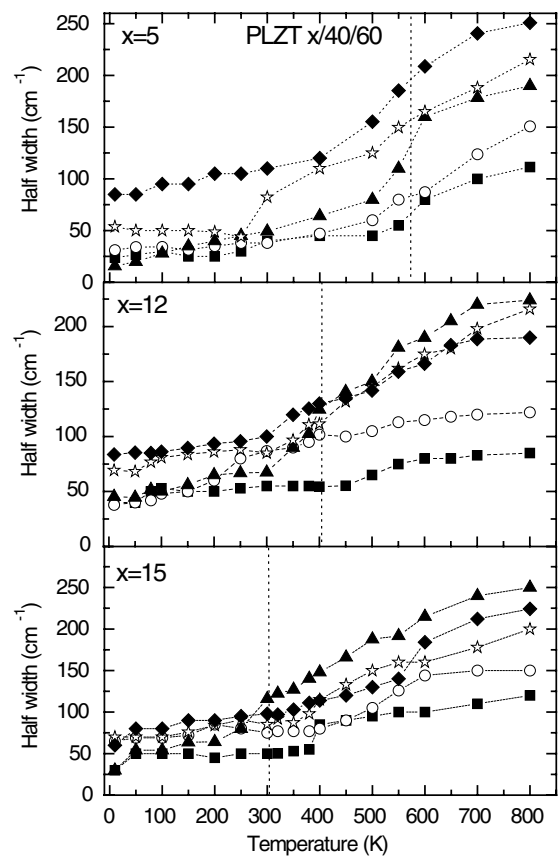


**Figure 4.** Temperature dependences of half-widths for the main bands in PLZT 5/40/60, 12/40/60 and 15/40/60. (Squares:  $110\text{ cm}^{-1}$ , circles:  $200\text{ cm}^{-1}$ , triangles:  $320\text{ cm}^{-1}$ , stars:  $550\text{ cm}^{-1}$ , diamonds:  $790\text{ cm}^{-1}$ .)

higher La content. In PLZT 5/40/60 it is still seen as a shoulder. Therefore we believe that it is related to the presence of lanthanum in the lattice, despite its high frequency. In all the samples a central mode component develops below  $800\text{ K}$  in unreduced spectra on approaching the ferroelectric phase transition and below it. This made it very difficult to fit the lowest mode, which is overdamped. From the Raman experiment it was not possible to deduce directly its frequency. Since such a mode was detected also in our THz experiment [14] and it was assigned to the overdamped  $E(\text{TO}_1)$  soft mode, we fixed its frequency (below  $20\text{ cm}^{-1}$ ) in accordance with the previous IR fit [15].

In figure 4 the temperature dependence of half-widths of the main bands, corresponding to the damping of the oscillators, is depicted for all three samples. On cooling, each mode splits and the damping and strength is redistributed among all developing modes. We assigned its strength and damping to the strongest of them. Damping constants therefore decrease on cooling, due to this effect and owing to the loss of anharmonicity of the vibrations. The respective  $T_C$  for the samples are marked by dotted lines.

The temperature dependence of the integrated strengths (corresponding band areas) of the main bands is shown in figure 5. First, the strength was integrated over the whole spectra (black stars). The total areas over the entire spectra stay reasonably constant for all samples, as expected. To

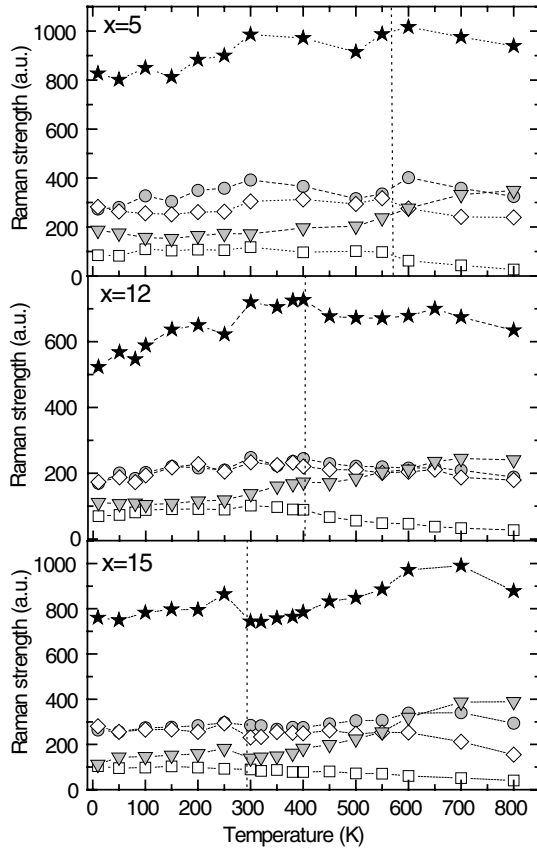


**Figure 5.** Temperature dependences of the Raman strengths of the four main spectral regions for PLZT 5/40/60, 12/40/60 and 15/40/60. (Squares: 0–100 cm<sup>-1</sup>, circles: 100–400 cm<sup>-1</sup>, diamonds: 400–700 cm<sup>-1</sup>, triangles: 700–900 cm<sup>-1</sup>, stars: total strength.)

investigate a possible transfer of energies we plot also the strength over four zones in the spectra (open symbols). The first zone corresponds to frequencies lower than 100 cm<sup>-1</sup>, where the central peak and the overdamped soft mode appear; the other three correspond to the three strong bands seen in the cubic phase (around 300, 500 and 750 cm<sup>-1</sup>). These bands split on cooling but their overall strength remains almost constant. The first zone (integrated over 0–100 cm<sup>-1</sup>) increases in strength a little due to the appearance of the central mode in the spectra and due to the hardening of the E(TO1) mode which enters in the spectra. The second band (integrated over 100–400 cm<sup>-1</sup> and where the main TO2 modes appear) shows a weak temperature dependence due to the mode at 300 cm<sup>-1</sup> which splits in two at  $T_C$ , corresponding to A<sub>1</sub>(TO2) and B<sub>1</sub> (see the discussion below). The highest-frequency band (above 700 cm<sup>-1</sup>) weakens more pronouncedly on cooling. This band corresponds to oxygen vibrations and LO3 modes, although inspection of individual strengths shows that it is the highest-frequency mode above 800 cm<sup>-1</sup> (known in the literature as the O breathing mode) which loses its strength. This behaviour is common to all three samples.

### 3.2. The EMA model

The temperature dependences of the IR spectra of PLZT  $x/40/60$  were published in [13, 14]. There we used a

generalized four-parameter oscillator model to fit the spectra and obtained the effective dielectric function  $\epsilon_{\text{eff}}(\omega)$ . In our last work [15] devoted to PLZT 15/40/60, we demonstrated that using EMA it is possible to calculate the local dielectric anisotropy and assign the mode symmetries in the THz and IR ranges, when polar grains or nanoclusters are present in ceramics. In this case, permittivity is different along and perpendicular to the local polarization in grains and different polar phonons are activated in the IR spectra with polarization along (A<sub>1</sub> modes) and perpendicular (E modes) to cluster polarization. Within this model the reflectivity is calculated as

$$R(\omega) = \left| \frac{\sqrt{\epsilon_{\text{eff}}(\omega)} - 1}{\sqrt{\epsilon_{\text{eff}}(\omega)} + 1} \right|^2, \quad (1)$$

where the effective dielectric function is derived from Bruggeman’s formula [17]:

$$\frac{2}{3} \frac{\epsilon_{\perp}(\omega) - \epsilon_{\text{eff}}(\omega)}{\epsilon_{\perp}(\omega) + 2\epsilon_{\text{eff}}(\omega)} + \frac{1}{3} \frac{\epsilon_{\parallel}(\omega) - \epsilon_{\text{eff}}(\omega)}{\epsilon_{\parallel}(\omega) + 2\epsilon_{\text{eff}}(\omega)} = 0. \quad (2)$$

The components of the dielectric tensor are calculated using the factorized form for the damped harmonic oscillators model [18]:

$$\epsilon_{\parallel,\perp}(\omega) = \epsilon_{\infty\parallel,\perp} \prod_{j=1}^n \frac{\omega_{\text{LO}j\parallel,\perp}^2 - \omega^2 + i\omega\gamma_{\text{LO}j\parallel,\perp}}{\omega_{\text{TO}j\parallel,\perp}^2 - \omega^2 + i\omega\gamma_{\text{TO}j\parallel,\perp}}. \quad (3)$$

The anisotropy of the high-frequency dielectric tensor is presumably negligible so that both principal components were set equal:  $\epsilon_{\infty\parallel} = \epsilon_{\infty\perp}$ .

For tetragonal PLZT samples with a parent cubic structure, the frozen polarization induces anisotropy inside the polar nanoregions and each cubic triplet F<sub>1u</sub> splits into A<sub>1</sub> + E pairs. Therefore,  $\epsilon_{\parallel}(\omega)$  is determined by the dielectric contribution from the A<sub>1</sub> modes and  $\epsilon_{\perp}(\omega)$  by the E modes. More details of the model and procedure can be found in [17].

In figure 6 we show the IR reflectivity spectra of PLZT 5/40/60 and 12/40/60, at RT and 20 K, respectively, together with the EMA fit. Parameters of the modes are listed in table 1 (the E(TO1) mode parameters are taken from the THz experiment). As in PLZT 15/40/60 [15], more IR modes than allowed by the tetragonal symmetry are detected: twelve modes in PLZT 5/40/60, instead of seven. There is a splitting of the three main perovskite TO modes. The dielectric spectra obtained from the fit are depicted in figure 7. Arrows mark longitudinal frequencies of the three main perovskite modes at the zeros of the permittivity and the transverse frequencies are marked at the corresponding maxima in the dielectric losses. The thicker solid curves represent the effective permittivity and the losses. E-symmetry modes give a higher contribution to the dielectric function. Permittivity arising from the E modes at low frequencies is higher than 500, whereas that from the A<sub>1</sub> modes is about 30. This large anisotropy is characteristic of all PZT and PLZT compounds, due to the presence of a strong E-symmetry soft mode below 30 cm<sup>-1</sup>.

**Table 1.** Frequencies ( $\omega_T, \omega_L$ ) and dielectric strengths ( $\Delta\epsilon$ ) of IR modes in PLZT 12/40/60 and 5/40/60 at characteristic temperatures in the tetragonal phase using the EMA model (equations (1)–(3)). Transverse and longitudinal frequencies ( $\omega_T$  and  $\omega_L$ ) are given in  $\text{cm}^{-1}$ . Asterisks denote parameters calculated from the THz experiment.

| Symmetry              | PLZT 12/40/60<br>$\epsilon_\infty = 6.12$ |            |                  |            |            |                  | PLZT 5/40/60<br>$\epsilon_\infty = 6.57$ |            |                  |            |            |                  |            |            |                  |
|-----------------------|---|------------|------------------|------------|------------|------------------|--|------------|------------------|------------|------------|------------------|------------|------------|------------------|
|                       | 20 K                                      |            |                  | 300 K      |            |                  | 20 K                                     |            |                  | 300 K      |            |                  | 500 K      |            |                  |
|                       | $\omega_T$                                | $\omega_L$ | $\Delta\epsilon$ | $\omega_T$ | $\omega_L$ | $\Delta\epsilon$ | $\omega_T$                               | $\omega_L$ | $\Delta\epsilon$ | $\omega_T$ | $\omega_L$ | $\Delta\epsilon$ | $\omega_T$ | $\omega_L$ | $\Delta\epsilon$ |
| A <sub>1</sub> (1)    | 107                                       | 158        | 14               | 107        | 145        | 10               | 122                                      | 166        | 11               | 112        | 165        | 18               | 113        | 150        | 10               |
| A <sub>1</sub> (2)    | 342                                       | 349        | 1.0              |            |            |                  | 349                                      | 360        | 1.7              | 340        | 367        | 3.8              | 336        | 343        | 2.4              |
|                       | 375                                       | 416        | 1.9              | 378        | 416        | 2.4              | 384                                      | 450        | 2.3              | 380        | 435        | 1.0              | 371        | 421        | 2.1              |
| A <sub>1</sub> (3)    | 588                                       | 720        | 2.5              | 580        | 721        | 2.8              | 625                                      | 717        | 1.5              | 602        | 722        | 1.9              | 579        | 705        | 2.3              |
| E(1)                  | 25  | 42         | 140*             | 10*        | 37         | 600*             | 41                                       | 61         | 250              | 22*        | 45         | 520*             | 17*        | 45         | 2000*            |
|                       | 70  | 121        | 79               | 70         | 121        | 88               | 63                                       | 66         | 3.2              | 73         | 120        | 17               | 77         | 121        | 59               |
|                       |   |            |                  |            |            |                  | 87                                       | 123        | 27               |            |            |                  |            |            |                  |
| E(2)                  | 188                                       | 215        | 21               | 190        | 223        | 27               | 201                                      | 229        | 21               | 200        | 233        | 22               | 194        | 233        | 27               |
|                       | 226                                       | 440        | 7.2              | 227        | 435        | 2.1              | 235                                      | 417        | 3.5              | 238        | 421        | 2.9              | 234        | 422        | 0.2              |
| E(4) + B <sub>1</sub> | 311                                       | 307        | 0.4              | 323        | 318        | 0.4              | 304                                      | 303        | 0.1              | 301        | 301        | 0.1              | 280        | 278        | 0.3              |
| E(3)                  | 540                                       | 693        | 1.5              | 534        | 690        | 1.7              | 519                                      | 532        | 0.6              | 520        | 532        | 0.6              | 525        | 680        | 1.6              |
|                       |   |            |                  |            |            |                  | 561                                      | 685        | 1.1              | 555        | 686        | 1.1              |            |            |                  |

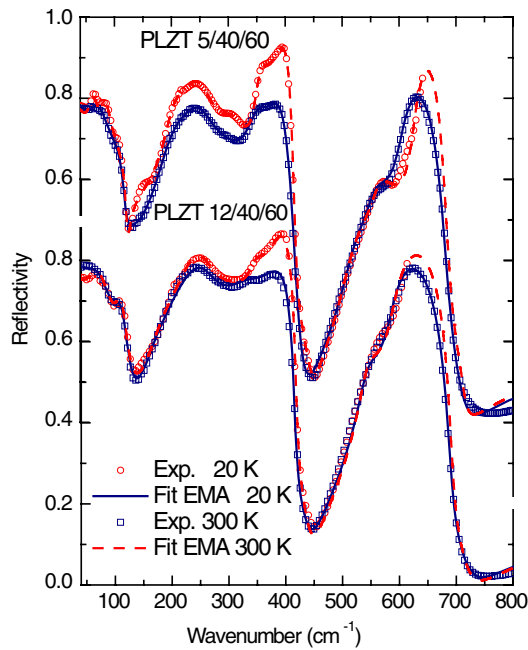


**Figure 6.** IR reflectivity spectra and their EMA fits for PLZT 5/40/60 and 12/40/60. Spectra at 20 K are cut above  $600 \text{ cm}^{-1}$  due to the use of polyethylene windows in the cryostat.

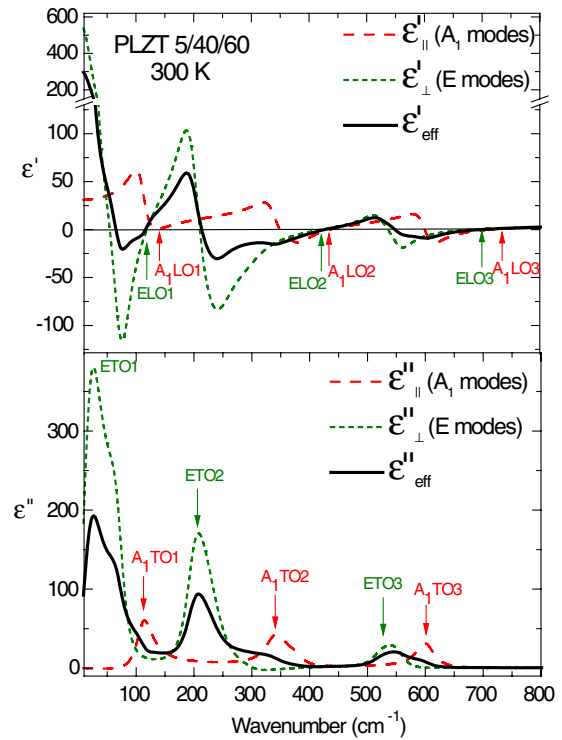


**Figure 7.** Permittivity and dielectric losses obtained from the EMA fit for PLZT 5/40/60 at room temperature.

## 4. Discussion

### 4.1. Structure symmetry considerations

The lattice dynamics of PLZT has been usually explained using group-theoretical results valid for simple cubic perovskites  $\text{ABO}_3$ : Raman activity is forbidden in the cubic group  $Pm\bar{3}m$  and there are three IR-active  $F_{1u}$  modes. When these compounds undergo a phase transition to a tetragonal phase,  $P4mm-C_{4v}^1$ , like  $\text{PbTiO}_3$ , the cubic triplets split into  $A_1 + E$  modes [19]. This analysis is valid on the assumption of a perfect structure without disorder. But PZT and PLZT

are samples with a high degree of disorder. To discuss the influence of disorder in the Raman- and IR-active modes, factor-group analysis for cubic and tetragonal phases taking into account different cation arrangements is shown in table 2.

In the cubic paraelectric phase a simple analysis, based on placing Pb in the  $1a$  site and taking Ti and Zr as one effective atom in the  $1b$  site, leads to three IR-active modes (plus an acoustic and a silent one, see table 2) at the Brillouin zone centre, which is not sufficient to

**Table 2.** Factor-group analysis of phonons in PLZT  $x/40/60$ , taking into account different atomic positions or unit cell doubling.  $Z_p = 2$  refers to the primitive unit cell. The conventional (centred) unit cell is four times bigger.

| Cubic ( $m3m$ )      |                        |   |                          |   |  |   |  |   |  |  |
|----------------------|------------------------|---|--------------------------|---|--|---|--|---|--|--|
| Atom                 | Pb ordered ( $Z = 1$ ) |   | Pb ordered ( $Z_p = 2$ ) |   | Pb/La off-site + Zr,Ti separated ( $Z = 1$ ) |   |  |   | Pb/La off-site + Zr, Ti off-site and separated ( $Z = 1$ ) |  |
|                      | Site                   | Represent.  | Site                     | Represent.  | Site   | Represent.  | Site   | Represent.  | Site   | Represent.   |
| Pb                   | $1a$                   | $F_{1u}$  | $8c$                     | $F_{1u} + F_{2g}$   | $8g$   | $2F_{1u} + 2F_{2g+E_g} + A_{1g}$  | $8g$   | $2F_{1u} + 2F_{2g+E_g} + A_{1g}$  | $8g$   | $2F_{1u} + 2F_{2g+E_g} + A_{1g}$   |
| La                   |                        |   |                          |   |  | $+F_{1g} + F_{2u} + E_u + A_{2u}$   |  | $+F_{1g} + F_{2u+E_u} + A_{2u}$   | $6e$   | $+F_{1g} + F_{2u+E_u} + A_{2u}$  |
| Ti                   | $1b$                   | $F_{1u}$  | $4b$                     | $F_{1u}$  | $1b$   | $F_{1u}$  | $6e$   | $2F_{1u} + F_{2g} + E_g + A_{1g}$   | $6e$   | $2F_{1u} + F_{2g} + E_g + A_{1g}$  |
| Zr                   |                        |   | $4a$                     | $F_{1u}$  | $1b$   | $F_{1u}$  | $6e$   | $+F_{1g} + F_{2u}$  | $6e$   | $+F_{1g} + F_{2u}$   |
| O <sub>1</sub>       |                        |   |                          |   |  |   |  | $2F_{1u} + F_{2u}$  | $3c$   | $2F_{1u} + F_{2u}$   |
| O <sub>2</sub>       | $3c$                   | $2F_{1u} + F_{2u}$                                      | $24e$                    | $2F_{1u} + F_{2g} + E_g + A_{1g} + F_{1g} + F_{2u}$   | $3c$   | $2F_{1u} + F_{2u}$  | $3c$   | $2F_{1u} + F_{2u}$  | $3c$   | $2F_{1u} + F_{2u}$   |
| Total                |                        | $4F_{1u}(\text{IR}) + F_{2u}(-)$                        |                          | $5F_{1u}(\text{IR}) + 2F_{2g}(\text{R}) + E_g(\text{R}) + A_{1g}(-) + F_{1g}(\text{R}) + F_{2u}(-)$ |  | $6F_{1u}(\text{IR}) + 3F_{2g}(\text{R}) + E_g(\text{R}) + A_{1g}(-) + F_{1g}(\text{R}) + 2F_{2u}(-) + E_u(-) + A_{2u}(-)$ |  | $6F_{1u}(\text{IR}) + 3F_{2g}(\text{R}) + E_g(\text{R}) + A_{1g}(-) + F_{1g}(\text{R}) + 2F_{2u}(-) + E_u(-) + A_{2u}(-)$ |  | $8F_{1u}(\text{IR}) + 4F_{2g}(\text{R}) + 3E_g(\text{R}) + 3A_{1g}(-) + 3F_{1g}(\text{R}) + 4F_{2u}(-) + E_u(-) + A_{2u}(-)$ |
| Activity             |                        | $3(\text{IR})$  |                          | $4(\text{IR}) + 4(\text{R})$  |  | $5(\text{IR}) + 4(\text{R})$  |  | $5(\text{IR}) + 4(\text{R})$  |  | $7(\text{IR}) + 10(\text{R})$  |
| Tetragonal ( $4mm$ ) |                        |   |                          |   |  |   |  |   |  |  |
| Atom                 | Pb ordered ( $Z = 1$ ) |   | Pb ordered ( $Z_p = 2$ ) |   | Pb/La off-site ( $Z = 1$ )                   |   | Pb/La off-site + Zr,Ti separated ( $Z = 1$ ) |   | Pb/La off-site + Zr,Ti off-site and separated ( $Z = 1$ )  |  |
|                      | Site                   | Represent.  | Site                     | Represent.  | Site   | Represent   | Site   | Represent.  | Site   | Represent.   |
| Pb                   | $1a$                   | $A_1 + E$   | $4b$                     | $A_1 + 2E + B_1$  | $4d$   | $2A_1 + 3E + B_1 + 2B_2 + A_2$  | $4d$   | $2A_1 + 3E + B_1 + 2B_2 + A_2$  | $4d$   | $2A_1 + 3E + B_1 + 2B_2 + A_2$   |
| La                   |                        |   |                          |   |  |   |  |   |  |  |
| Ti                   | $1b$                   | $A_1 + E$   | $2a$                     | $A_1 + E$   | $1b$   | $A_1 + E$   | $1b$   | $A_1 + E$   | $4e$   | $2A_1 + 3E + 2B_1 + B_2 + A_2$   |
| Zr                   |                        |   | $2a$                     | $A_1 + E$   | $1b$   | $A_1 + E$   | $1b$   | $A_1 + E$   | $4e$   | $2A_1 + 3E + 2B_1 + B_2 + A_2$   |
| O <sub>1</sub>       | $1b$                   | $A_1 + E$   | $2 \times 2a$            | $2A_1 + 2E$   | $1b$   | $A_1 + E$   | $1b$   | $A_1 + E$   | $1b$   | $A_1 + E$  |
| O <sub>2</sub>       | $2c$                   | $A_1 + 2E + B_1$  | $8c$                     | $2A_1 + 3E + B_1 + 2B_2 + A_2$  | $2c$   | $A_1 + 2E + B_1$  | $2c$   | $A_1 + 2E + B_1$  | $2c$   | $A_1 + 2E + B_1$   |
| Total                |                        | $4A_1(\text{R, IR}) + 5E(\text{R, IR}) + B_1(\text{R})$ |                          | $7A_1(\text{R, IR}) + 9E(\text{R, IR}) + 2B_1(\text{R}) + 2B_2(\text{R}) + A_2(-)$                  |  | $5A_1(\text{R, IR}) + 7E(\text{R, IR}) + B_1(\text{R}) + 2B_2(\text{R}) + A_2(-)$   |  | $6A_1(\text{R, IR}) + 8E(\text{R, IR}) + 2B_1(\text{R}) + 2B_2(\text{R}) + A_2(-)$  |  | $8A_1(\text{R, IR}) + 12E(\text{R, IR}) + 6B_1(\text{R}) + 4B_2(\text{R}) + 3A_2(-)$   |
| Activity             |                        | $7(\text{R, IR}) + 1(\text{R})$                         |                          | $14(\text{R, IR}) + 4(\text{R})$  |  | $10(\text{R, IR}) + 3(\text{R})$  |  | $12(\text{R, IR}) + 4(\text{R})$  |  | $18(\text{R, IR}) + 13(\text{R})$  |

account for the IR and Raman modes detected in the experiments. Our IR experiments [14] showed seven IR modes above the Burns temperature  $T_d \sim 680$  K [20]. The Raman experiment shows seven modes up to 800 K for PLZT 15/40/60 (see figure 3) and six modes for PLZT 5/40/60.

The presence of a Raman signal in the cubic phase, which is a well-known effect in many cubic perovskites, speaks in favour of the symmetry breakdown at micro-or nanoscopic scales. Our results confirm the lowering of local symmetry in the cubic phase, even if our samples are macroscopically cubic at high temperatures (above 700 K), as well as found for Ti-rich PZT [21]. El Marssi *et al* attributed the presence of a Raman signal in the cubic phase of PLZT to fluctuations of the polarization [9]. Our data show that the Raman signal is of first order and can be assigned to the breakdown of cubic symmetry in nanoregions. The laser spot, a few micrometres in diameter, measures over an ensemble of nanometric clusters in which polarization is already developed; therefore it is averaged as in the fluctuating model [9]. However, the simple model of modes arising from polar nanoregions where tetragonal symmetry is already developed cannot explain spectra above the Burns temperature where these regions are still not developed. Therefore another explanation should be found to account for the modes above  $T_d$ . Also the activation of the silent  $F_{2u}$  mode due to symmetry breaking in nanoclusters is not enough to account for the seven IR modes found.

A second mechanism which could be responsible for the activation of Raman modes in the cubic phase is a local unit cell doubling, due to ordering in B-site cations. Rhombohedral lead-based perovskite relaxors with two B atoms show often locally doubled cell structures. In PLZT  $x/40/60$  the doubling could be induced by a Ti/Zr arrangement, which is almost in a 50/50 ratio. But it was shown by Mihajlova *et al* [22] that Raman spectra present in the cubic phase ( $Fm\bar{3}m$ ) are not explained just by the doubling of the unit cell; additional peaks were assigned to structural distortions and cation shifts in  $Pb(Sc_{0.5}Ta_{0.5})O_3$ . In table 2 it is shown that this effect leads to four IR-and four Raman-active modes, which again is not enough to explain our results. The group analysis shows that the motion of Pb and O atoms is responsible for the Raman-active modes, but not that of Ti/Zr. Following Mihajlova *et al*, indications of the unit cell doubling are a low-frequency mode attributed to Pb and a high-frequency B–O stretching mode above 800  $cm^{-1}$ . In PZT and PLZT both modes are present, with high damping constants. Therefore doubling could exist at a local scale, although some other cause must be found for the presence of Raman and IR bands in the middle-frequency part. It is worth noting that the latter mode, although it seems to be related to the B-site ordering [23] in many complex perovskites, was also found in  $Ca(Zr_xTi_{1-x})O_3$  even in the absence of a B arrangement [24]. So the question is still open.

An important aspect of lead-containing perovskites is that the Pb atom is substantially anharmonic and Pb disorder is fundamental in the dielectric behaviour of these compounds. A diagonal off-site Pb atom was recently discovered by high energy synchrotron radiation diffraction [25]. If Pb atoms were placed in  $8g(x, x, x)$  sites, they would contribute to the  $Pm\bar{3}m$  group with  $2F_{1u}(IR) + 2F_{2g}(R) + E_g(R) + A_{1g}(R) +$

$F_{1g}(-) + F_{2u}(-) + E_u(-) + A_{2u}(-)$  modes. If moreover we consider Ti and Zr as two separate atoms (not an effective one) at the  $1b$  sites, each of them contributes with one  $F_{1u}$  mode. This is supported by the large difference in mass of the two atoms, which induces different frequencies in the  $F_{1u}$  mode. In this case we would have in total five IR-and four Raman-active modes (see table 2). This is not enough to explain the IR and Raman data in the cubic phase, because Pb cannot give mode frequencies as high as 500 or 700  $cm^{-1}$ , but it shows that a small off-site position of atoms in the perovskite lattice can activate new IR and Raman modes that are forbidden without taking into account the disorder in the standard factor-group analysis.

A possible explanation for the middle-frequency modes could be the off-site position of B atoms. Zr and Ti are displaced in the ferroelectric phase in PZT samples near the morphotropic phase boundary (MPB). Ti-rich PZT shows distortions of B cations along the (100) direction of about 0.3 Å at RT [26]. If Ti and Zr atoms showed similar off-site behaviour in the cubic phase, they would be placed in  $6e$  sites  $(x, 0, 0)$ , contributing with  $2F_{1u}(IR) + F_{2g}(R) + E_g(R) + A_{1g}(R) + F_{1g}(-) + F_{2u}(-)$  modes. The total number of active modes would be then seven IR and ten Raman (see table 2). The number of IR-active modes agrees with our results (we fitted seven cubic IR modes at 800 K in our three PLZT  $x/40/60$ ).

Taking a look to the cubic Raman spectra (figures 1 and 2) three strong bands are seen: near 300, 550 and 750  $cm^{-1}$ . PLZT 15/40/60 and 12/40/60 samples show also a mode at  $\omega \sim 640$   $cm^{-1}$ , absent in PLZT 5/40/60 at high temperatures. Additionally, two weaker bands are present at lower frequencies ( $\omega \sim 60, 120$   $cm^{-1}$ ). There are seven Raman modes in total, in agreement with the group analysis for off-site cations. Even if the number of allowed Raman modes is higher (10), some modes can be too weak to be detected or hidden in the spectra due to the high damping of the vibrations. The possibility of unit cell doubling due to B-site ordering allows just four Raman modes in the cubic phase. Therefore a combinations of the two effects could be possible too.

Similar considerations can be applied to the tetragonal phase. If we take the pure tetragonal  $PbTiO_3$  and atoms at the ideal sites: Pb in  $1a$ , Ti and O in  $1b$  and  $2c$ , we obtain the  $3A_1(R, IR) + 4E(R, IR) + 1B_1(R)$  optic modes (see table 2). This analysis was used also for the mixed compounds,  $Pb(Zr_xTi_{1-x})O_3$  (PZT) [27] and PLZT [28], and the expected number of modes was considered the same. However, a small planar displacement shifts the atom to a more general site  $4d(x, x, 0)$  with a statistical partial occupancy of 1/4, which has been suggested for PZT by Noheda *et al* using XRD [29], and by Frantti *et al* using neutron scattering [30]. Our XRD measurements in PLZT 12/40/60 also agree with this suggestion [15]. An atom in a  $4d$  site gives rise to the following modes:  $2A_1(R, IR) + A_2(-) + B_1(R) + 2B_2(R) + 3E(R, IR)$ . The factor-group analysis taking this fact into account leads to ten simultaneously IR-and Raman-active modes and three pure Raman-active modes (see table 2). As the multiplicity of the

Pb site is higher, there are more effective atoms in the unit cell and the number of total modes is higher, which is in better agreement with the IR and Raman experimental results. However, Pb off-site is not sufficient to account for some extra high-frequency modes. If, besides, we take into account Zr and Ti separately as two independent atoms, and not as an effective one, there is another extra  $1b$  site contributing with an ( $A_1 + E$ ) pair of modes and this leads to twelve simultaneously IR- and Raman-active modes and four Raman-active modes (see table 2).

Another possibility for PZT is to leave Pb in the  $1a$  site, but consider the doubling of the unit cell due to locally ordered Zr/Ti distribution. From the doubled cubic cell (space group  $Fm\bar{3}m$ ) the tetragonal ferroelectric phase can be attained by the group-subgroup sequence ( $Fm\bar{3}m > I4/mmm > I4mm$ ), with fourteen modes simultaneously IR- and Raman-active and four Raman-active modes (see details in table 2). This possibility requires local ordering in the arrangement of Zr and Ti atoms, which was not observed up to now. The ordering could be settled in the nanoscopic scale and therefore not detectable by XRD, although detectable in Raman or IR spectroscopy. The situation with anharmonic Pb atoms seems to be, however, more realistic.

Recently, a dynamical disorder in the B position and shifts of Zr/Ti atoms were found in PZT near the MPB [26]. Allowing for some disorder between Zr and Ti atoms in the (100) direction, which is the most probable for Ti-rich PZTs, we have other two extra  $4e$  ( $x, 0, z$ ) sites, which leads to 18 (IR,R) and 13 (R) active modes (see table 2).

The twelve IR modes fitted by the EMA model in the tetragonal phase of PLZT 5/40/60 seem to agree with the model of Pb disorder and Zr and Ti as two separate atoms. Probably the shifts in Zr and Ti in our compositions are not as pronounced as in the samples closer to the MPB [26] and therefore our XRD measurements did not detect it [15]. Raman results in the tetragonal phase (26 modes at low temperatures) seems to agree also with the analysis, but the situation in Raman spectra is more complicated owing to the presence of TO and LO components and possible mixing of symmetries in ceramics. Therefore, assignment of symmetries should be done before making any quantitative estimation.

#### 4.2. Assignment of mode symmetries

In order to identify E and  $A_1$  symmetries which are simultaneously IR- and Raman-active, we plot the IR frequencies fitted by the EMA model together with the Raman frequencies fitted by damped harmonic oscillators in figure 8. We have to take into account that in ceramics we do not observe pure transverse and longitudinal modes, but a mixture of both, so that one can expect deviations by several  $\text{cm}^{-1}$  in frequencies from those from IR data, not considering the accuracy of the IR data due to the experimental errors and the EMA approach. Bearing this in mind we labelled most of the  $A_1$  and E-symmetry Raman modes according to the nearest IR modes (results from table 1). In table 3 we show the comparison of our previous results [14] with the EMA model and the Raman experiment for PLZT 5/40/60 and 15/40/60 at low temperature. The distinction between

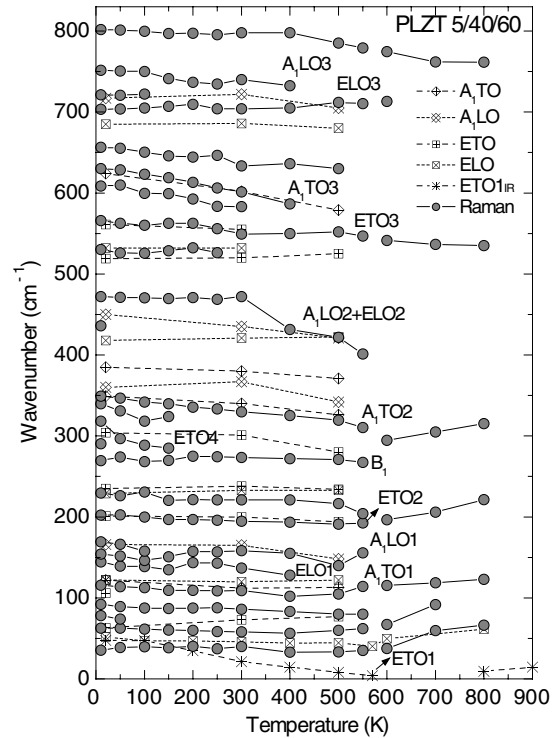


**Figure 8.** Raman frequencies (solid) compared to the IR frequencies taken from the EMA model (crosses). Assignment of the symmetries is valid for the tetragonal ferroelectric phase.

the TO and LO character of a Raman peak can be inferred already from the four-parameter model fitting for vibrations which are simultaneously Raman- and IR-active, but the EMA model provides also the type of symmetry. In general, the frequencies agree reasonably well, also with the results for PZT [12]. The three main E and  $A_1$ -symmetry bands are in agreement with the prototypical modes in  $\text{PbTiO}_3$ . The only difference is the assignment of the  $A_1$ (TO1) mode to the line at  $110 \text{ cm}^{-1}$  instead of the one at  $150 \text{ cm}^{-1}$ . Our assignment comes from the fit of the reflectivity, in which  $A_1$  modes are taken as the stiffened components of the split cubic  $F_{1u}$  modes since they appear as shoulders in the high-frequency part of each IR mode. The identification of the soft E(TO1) mode in the Raman spectra is difficult because it is split in two heavily damped low-frequency excitations in the THz range [14, 21]. In the Raman spectra we see an overdamped low-frequency excitation, but the superposition of the Rayleigh wing at low frequencies precludes evaluation of its parameters. The lowest observable Raman mode at about  $30 \text{ cm}^{-1}$  (at 10 K) could correspond to the overdamped TO component of the lowest E-symmetry mode fitted with the EMA model, but also to an E(LO) component (see figure 8). The mode at  $70 \text{ cm}^{-1}$  is an E(TO) mode and probably stems from the same  $F_{1u}$  mode. In table 3 there are unassigned Raman modes for PLZT 5/40/60 at  $154, 640$  and  $730 \text{ cm}^{-1}$  and at the highest-frequency  $\sim 820 \text{ cm}^{-1}$ , because they have no IR equivalent. These modes could be of  $B_2$  symmetry. Additional weak modes at  $340$  and  $609 \text{ cm}^{-1}$  can be split from the  $A$ (TO2) and  $A$ (TO3) modes.

In general, Raman and IR results at low temperatures show that all main modes (stemming from the ordered tetragonal

**Table 3.** Comparison of the polar modes frequencies (in  $\text{cm}^{-1}$ ) between PLZT 5/40/60 and PLZT 15/40/60, obtained from the fit of the IR reflectivity by the generalized four-parameter oscillator model [14], the effective-medium approximation (EMA) model [15] at 20 K and the fit of the Raman spectra by damped oscillators at 10 K. GR stands for geometrical resonances, i.e. modes created by resonances between two LO or TO modes of different symmetries in the IR spectra.

| Symmetry             | PLZT 5/40/60    |               |                 | PLZT 15/40/60   |               |                 |
|----------------------|-----------------|---------------|-----------------|-----------------|---------------|-----------------|
|                      | 4-par<br>(20 K) | EMA<br>(20 K) | Raman<br>(10 K) | 4-par<br>(20 K) | EMA<br>(20 K) | Raman<br>(10 K) |
| E(TO1)*              | 47              | 41            | 35.6            | 22.8            | 30            | 28              |
| E(LO)                | 52              | 61            |                 | 28.8            | 51            |                 |
| E(TO)                | 63              | 63            | 62.6            | 60.9            | 70            | 64              |
| E(LO)                | 70.8            | 66            | 78              |                 |               |                 |
| E(TO)                | 80              | 87            | 92              |                 |               | 87.4            |
| GR                   | 98.4            |               |                 | 106.9           |               |                 |
| A <sub>1</sub> (TO1) | 108.8           | 122           | 115.8           | 108.9           | 108           | 108.6           |
| E(LO1)               | 119.7           | 123           | 144.5           | 122.8           | 119           | 141.3           |
|                      |                 |               | 154.1           |                 |               | 167.5           |
| GR                   | 154             |               |                 |                 |               |                 |
| A <sub>1</sub> (LO1) | 157.4           | 166           | 169.3           |                 | 201           | 206.9           |
| E(TO2)               | 201.5           | 201           | 202.4           | 201.0           | 186           | 236.7           |
| E(LO)                | 217.9           | 229           |                 | 229.8           | 223           |                 |
| E(TO)                | 226.0           | 235           | 229.4           | 230.0           | 225           |                 |
| B <sub>1</sub>       |                 |               | 269.5           |                 |               | 275.9           |
| E(LO4)               | 299.8           | 303           | 290.5           | 301.0           | 309           |                 |
| E(TO4)               | 303.6           | 304           | 318.4           | 305.3           | 318           | 316.1           |
| GR                   | 332             |               |                 | 329.4           |               |                 |
| A <sub>1</sub> (TO)  |                 |               | 339.6           |                 |               |                 |
| A <sub>1</sub> (TO2) | 345             | 349           | 349.0           | 332.4           | 338           | 328.1           |
| A <sub>1</sub> (LO)  | 371             | 360           |                 | 356.4           | 344           |                 |
| A <sub>1</sub> (TO)  | 383             | 384           |                 | 375.8           | 375           |                 |
| E(LO2)               | 419             | 417           | 435.6           | 420.5           | 416           |                 |
| GR                   | 438             |               |                 | 427.2           |               |                 |
| A <sub>1</sub> (LO2) | 444             | 450           | 471.9           | 443.1           | 441           | 457.6           |
| E(TO)                | 522             | 519           | 530.3           |                 |               | 535.4           |
| E(LO)                | 526             | 532           |                 |                 |               |                 |
| E(TO3)               | 545             | 561           | 565.9           | 538.9           | 538           | 563.0           |
| GR                   | 597             |               |                 | 597.7           |               |                 |
| A <sub>1</sub> (TO)  |                 |               | 608.7           |                 |               |                 |
| A <sub>1</sub> (TO3) | 606             | 624           | 630.3           | 600.5           | 580           | 590.3           |
|                      |                 |               | 656.4           |                 |               | 641.4           |
| E(LO3)               | 690             | 685           | 703.4           | 694.4           | 688           | 708.8           |
| GR                   | 698             |               |                 | 704.6           |               |                 |
|                      |                 |               | 721.4           |                 |               | 732.1           |
| A <sub>1</sub> (LO3) | 718             | 705           | 754.2           | 709.1           | 724           | 779.1           |
|                      |                 |               | 805.8           |                 |               | 822.5           |

structure) split on cooling. This was observed in PZT, too [12]. The splitting can be assigned to new modes appearing due to off-site positions of cations (which freeze at low temperatures), but also to the two-mode behaviour due to Ti and Zr atoms. For example, the frequency of the E(TO2) mode—stemming from the Slater mode (B–O<sub>6</sub> vibrations)—is  $\omega \sim 200 \text{ cm}^{-1}$  in PbZrO<sub>3</sub> and  $\omega \sim 230 \text{ cm}^{-1}$  in PbTiO<sub>3</sub>, in agreement with the two E(TO) modes fitted by the EMA model at 20 K. Similar splitting is seen in E(TO3), A(TO2) and A(TO3) modes.

Table 3 shows also that some frequencies present in the previous IR model are not present in the EMA model. This means that these extra modes are artefacts created by geometrical resonances (GR). They occur whenever there is a crossing of frequencies between modes of different

symmetries. Five of these resonances are present at low temperatures in the IR spectra of PLZT, at 99, 154, 332, 597 and  $698 \text{ cm}^{-1}$ . They look as small bumps in the spectra, and in the standard model they were fitted by very weak oscillators. The EMA fit can account for them without adding any weak oscillators.

### 4.3. Influence of La

It is known that the increase of La content in PLZT has two important effects: it reduces  $T_C$  and induces relaxor behaviour, decreasing the maximum of permittivity [2]. In addition it produces transparency by lowering the optical anisotropy. La<sup>3+</sup> has an ionic radius comparable to Pb<sup>2+</sup> ions and is incorporated in the tetragonal perovskite structure at the A sites. There are two possible ways of neutralizing the extra positive charge from the addition of La<sup>3+</sup>: by creation of either lead (A-site) or titanium (B-site) vacancies. Both are present in PLZT [31]. A third way—reduction from Ti<sup>4+</sup> to Ti<sup>3+</sup>—was not found up to now.

The appearance of new Raman modes on cooling is connected with the phase transition and symmetry lowering. Comparing its parameters at the same temperatures does not shed much light on the La influence because each sample is at a different distance from  $T_C$ . For instance, the fact that at lower temperatures PLZT 5/40/60 has a higher number of modes than PLZT 15/40/60 is due to PLZT 5/40/60 being further from  $T_C$  and the modes are better resolved. The cubic PLZT 15/40/60 and 12/40/60 show an extra mode at  $\sim 640 \text{ cm}^{-1}$ , absent in the sample with lower La content, which seems to indicate that it could be connected with La vibrations, despite its high frequency. If La induces Ti/Zr vacancies in the lattice, this can affect locally the vibrations of the surrounding oxygen octahedra at high frequencies. Oxygen atoms without one positive charge inside the octahedra will repel each other more, because of charge compensation, and the bonding will be weaker, showing lower frequency. In this way, the extra mode could be a secondary effect of the La doping. On cooling, this mode appears in PLZT 5/40/60 too (at 200 K as  $\omega \sim 650 \text{ cm}^{-1}$ , see figure 3). At higher percentage of La its strength is higher because there are more B-site vacancies.

## 5. Conclusions

The Raman spectra of PLZT  $x/40/60$  were measured from high temperatures down to 10 K and compared with previous IR data. The presence of increasing La doping does not affect much the aspect of the spectra except in the appearance at high temperatures of a mode around  $640 \text{ cm}^{-1}$  for  $x = 12$  and 15. At low frequencies a central mode develops below 800 K for all the samples on approaching the phase transition. This is related to the overdamped soft E(TO) mode at THz frequencies.

A new methodology was proposed to interpret the Raman spectra in polar ceramics. The effective medium approximation was used to fit the IR spectra in the ferroelectric phase where polar grains are present. In this way it is possible to assign the mode symmetries and compare simultaneously IR- and Raman-active modes.

A strong local dielectric anisotropy was found in the THz and IR ranges for all the samples, due to different IR-active modes polarized along and perpendicular to the polarization in grains and/or polar nanoregions. The strongest contribution to the permittivity is carried by the E-symmetry modes at the low-frequency part of the spectra. By comparison to IR data we could identify the symmetries of most of the Raman modes detected.

We performed a new factor-group analysis taking into account the off-site positions of cations in cubic and tetragonal as well as the chemical inhomogeneity. Anharmonicity of Pb and separate vibrations for Ti and Zr can account for the higher number of active optic modes detected in both phases.

In our previous paper we attributed the presence of extra IR modes in the cubic phase to the lowering of cubic symmetry to tetragonal in polar nanoclusters. But these should not be developed yet above the Burns temperature  $T_d \sim 680$  K. The presence of the extra IR and ‘forbidden’ Raman modes above 700 K can be explained as due to off-centre positions of cations and local unit cell doubling. This proves that anharmonicity plays an essential role in the lattice dynamics of these perovskites, and that IR and Raman techniques are sensitive to very small local deviations from the perfectly ordered structures.

## Acknowledgments

This work was supported by ASCR project IAA100100701, KAN301370701, GAČR 202/06/0403 and AVOZ10100520.

## References

- [1] Land C E, Thatcher P and Haertling G H 1974 Electrooptic ceramics *Advances in Materials and Device Research* vol 4 ed R Wolfe (New York: Academic) pp 137–233
- [2] Haertling G H 1987 *Ferroelectrics* **75** 25
- [3] Kersten O, Rost A and Schmidt G 1983 *Phys. Status Solidi a* **75** 495
- [4] Viehland D, Jang S and Wuttig M 1991 *J. Appl. Phys.* **69** 6595
- [5] Kamba S, Bovtun V, Petzelt J and Rychetsky I 2000 *J. Phys.: Condens. Matter* **12** 497
- [6] Dai X, Di Giovanni A and Viehland D 1993 *J. Appl. Phys.* **74** 3399
- [7] Dai X, Xu Z and Viehland D 1996 *Japan. J. Appl. Phys.* **79** 1021
- [8] Lurio A and Burns G 1974 *J. Appl. Phys.* **45** 1986
- [9] El Marssi M, Farhi R, Dai X, Morell A and Viehland D 1996 *J. Appl. Phys.* **80** 1079
- [10] El Marssi M, Farhi R and Viehland D 1997 *J. Appl. Phys.* **81** 355
- [11] Frantti J, Lantto V and Lappalainen J 1996 *J. Appl. Phys.* **79** 1065
- [12] Frantti J, Lappalainen J, Lantto V, Nishio S and Kakihana M 1999 *Japan. J. Appl. Phys.* **38** 5679
- [13] Buixaderas E, Nuzhnyy D, Veljko S, Savinov M, Vaněk P, Kamba S, Petzelt J and Kosec M 2006 *Phase Transit.* **79** 415
- [14] Buixaderas E, Nuzhnyy D, Veljko S, Kamba S, Savinov M, Petzelt J and Kosec M 2007 *J. Appl. Phys.* **101** 074106
- [15] Buixaderas E, Kamba S, Petzelt J, Drahokoupil J, Laukef F and Kosec M 2007 *Appl. Phys. Lett.* **91** 112909
- [16] Pokorný J, Petzelt J, Gregora I, Železný V, Vorlíček V, Zikmund Z, Fedorov I, Pronin A and Kosec M 1996 *Ferroelectrics* **186** 115
- [17] Hlinka J, Ostapchuk T, Noujni D, Kamba S and Petzelt J 2006 *Phys. Rev. Lett.* **96** 027601
- [18] Gervais F 1983 *Infrared and Millimeter Waves* vol 8 ed K J Button (New York: Academic) p 279
- [19] Freire J D and Katiyar R S 1988 *Phys. Rev. B* **37** 2074
- [20] Burns G and Dacol F H 1983 *Phys. Rev. B* **28** 2527
- [21] Ikeuchi Y, Kojima S and Yamamoto T 1997 *Japan. J. Appl. Phys.* **36** 2985
- [22] Mihajlova B, Bismayer U, Gutter B, Gospodinov M and Konstantinov L 2002 *J. Phys.: Condens. Matter* **14** 1091
- [23] Siny I G, Katiyar R S and Bhalla A S 1998 *J. Raman Spectrosc.* **29** 385
- [24] Levin I, Cockayne E, Lufaso M W, Woicik J C and Maslar J E 2006 *Chem. Mater.* **18** 854
- [25] Kuroiwa Y, Terado Y, Kim S J, Sawada A, Yamamura Y, Aoyagi S, Nishibori E, Sakata M and Takata M 2005 *Japan. J. Appl. Phys.* **44** 7151
- [26] Grinberg I, Cooper V R and Rappe A M 2004 *Phys. Rev. B* **69** 114118
- [27] Burns G and Scott B A 1970 *Phys. Rev. Lett.* **25** 1191
- [28] Brya W J 1971 *Phys. Rev. Lett.* **26** 1114
- [29] Noheda B, Gonzalo J A, Cross L E, Guo R, Park S E, Cox D E and Shirane G 2000 *Phys. Rev. B* **61** 8687
- [30] Frantti J, Ivanov S, Eriksson S, Rundlöf H, Lantto V, Lappalainen J and Kakihana M 2002 *Phys. Rev. B* **66** 064108
- [31] Hardtl K H and Hennings D 1972 *J. Am. Ceram. Soc.* **55** 230